Thermonuclear reaction rate of ^{56}Ni$(p,\gamma)^{57}$Cu and ^{57}Cu$(p,\gamma)^{58}$Zn

O. Forstner,[1,*] H. Herndl,[1] H. Oberhummer,[1] H. Schatz,[2,†] and B. A. Brown[3]
[1]*Institut für Kernphysik, Technische Universität Wien, Wiedner Hauptstraße 8–10, A-1040 Wien, Austria*
[2]*Gesellschaft für Schwerionenforschung, Planckstraße 1, D-64291 Darmstadt, Germany*
[3]*Department of Physics and Astronomy, and National Superconducting Cyclotron Laboratory, Michigan State University, East Lansing, Michigan 48824*
(Received 25 May 2001; published 30 August 2001)

Updated stellar rates for the reactions ^{56}Ni$(p,\gamma)^{57}$Cu and ^{57}Cu$(p,\gamma)^{58}$Zn are calculated by using all available experimental information as well as input data from the nuclear shell model. We calculated Coulomb and Thomas-Ehrmann shifts to obtain the unknown excitation energies and the spin/parity assignments of ^{58}Zn. The astrophysical consequences are discussed.

DOI: 10.1103/PhysRevC.64.045801 PACS number(s): 26.30.+k, 21.10.Jx, 25.40.Lw, 97.10.Cv

I. INTRODUCTION

The rp process is the dominating nuclear process in hot and explosive hydrogen burning scenarios [1–4]. The process is characterized by a large number of proton capture reactions and β decays. It is responsible for the energy production and nucleosynthesis in a variety of astrophysical sites with different temperature and density conditions like novae, x-ray bursts, x-ray pulsars, and maybe accretion disks around low mass black holes.

Ever since the rp process was introduced by Wallace and Woosley in 1981 the very special role of the doubly magic nucleus ^{56}Ni has been recognized. At the high temperature and density conditions in x-ray bursts and x-ray pulsars ^{56}Ni is a so called waiting point in the rp-process path. Waiting points are isotopes with a small or negative Q value for proton capture. In these cases proton capture is hampered by either photodisintegration or proton decay and the reaction flow has usually to wait for the relatively slow β decay. For ^{56}Ni the low proton capture Q value of 695 keV coincides with a low proton capture rate (owing to the low level density near the closed shell) and the extraordinary long β-decay lifetime. The long terrestrial half-life of 6.075 d [5] is considerably prolonged for the fully ionized atom at stellar conditions since the decay is dominated by electron capture [6,7]. In fact, ^{56}Ni is the only waiting point nucleus in the rp process which has a β-decay lifetime exceeding all typical processing time scales. Therefore, at ^{56}Ni the rp process either ends or has to proceed via proton captures. Most of the earlier studies assumed that the rp process ends at ^{56}Ni [1,8–10] or that at least processing beyond ^{56}Ni is negligible [11]. However, more recent studies based on larger reaction networks show that the rp process in x-ray bursts and x-ray pulsars proceeds well beyond ^{56}Ni [12–14] and can even reach the $A=80-100$ mass region [15–18]. This has far reaching consequences for the consumption of hydrogen and helium fuel as well as for the energy production and the final composition of the rp process ashes. This in turn is linked to a variety of neutron star properties and observables (see Schatz *et al.* [17] and references therein). However, these conclusions depend sensitively on the proton capture rates on ^{56}Ni and, when at high temperatures ^{56}Ni and ^{57}Cu are in (p,γ)-(γ,p) equilibrium, on ^{57}Cu.

For the ^{56}Ni$(p,\gamma)^{57}$Cu reaction several calculations have been performed in the past. A more recent estimate was made by Van Wormer *et al.* [13], but at that time only incomplete information about the level structure in ^{57}Cu was available. The situation improved considerably after Zhou *et al.* [19] remeasured the level structure of ^{57}Cu and evaluated an updated reaction rate. A first attempt to measure the spectroscopic factors of the low lying proton unbound states in ^{57}Cu was made by Rehm *et al.* [20] who populated the analogue states using the $d(^{56}\mathrm{Ni},^{57}\mathrm{Ni})p$ reaction in a radioactive beam experiment. Rehm *et al.* also presented a new shell model calculation for the ^{56}Ni$(p,\gamma)^{57}$Cu reaction rate and found, within the relatively large errors of the model dependent analysis, agreement between their calculated and measured spectroscopic factors. Although the spectroscopic factors are in agreement with Zhou *et al.* [19], the derived reaction rates differ substantially.

For the ^{57}Cu$(p,\gamma)^{58}$Zn reaction only a rate calculated with the statistical Hauser-Feshbach model is available [21]. However, this approach might be doubtful as in this case the level density in the compound nucleus is quite small.

We present a new analysis of the reactions ^{56}Ni$(p,\gamma)^{57}$Cu and ^{57}Cu$(p,\gamma)^{58}$Zn based on improved theoretical calculations combined with all available experimental data. In the shell model we used the most recent interaction from Ormand 1997 [22]. Proton widths were calculated using a folding potential. For experimentally unknown excitation energies and spin-parity assignments we calculated Coulomb and Thomas-Ehrman shifts to obtain the energies starting from the experimentally known levels in the mirror nuclei. Spectroscopic factors were calculated using the nuclear shell model. Gamma widths were obtained from the experimental information in the mirror nuclei.

In Sec. II we describe briefly the formalism for calculat-

*Present address: CERN, CH-1211 Genève 23, Switzerland.
†Present address: Department of Physics and Astronomy, and National Superconducting Cyclotron Laboratory, Michigan State University, East Lansing, MI 48824.

ing stellar reaction rates. The experimental and theoretical nuclear input parameters for the calculation of the reaction rates are presented in Sec. III. Results and astrophysical implications are discussed in Sec. IV. A summary is given in Sec. V.

II. CALCULATION OF STELLAR REACTION RATES

The proton capture cross sections on the investigated nuclei are predominantly determined by summing the contributions from isolated resonances corresponding to unbound compound nuclear states and from the nonresonant direct capture (DC) process. In the following we briefly describe the method of calculating the resonant and nonresonant (DC) contributions to the stellar reaction rates.

A. Resonant reaction contributions

For the reactions considered in this work the resonances are narrow and isolated. The resonant rate contribution can be calculated from resonance energies E_i and resonance strengths $(\omega\gamma)_i$ (both in units of MeV) [23]

$$N_A\langle\sigma v\rangle_r = 1.54\times 10^{11}(\mu T_9)^{-3/2}\sum_i (\omega\gamma)_i \times \exp(-11.605E_i/T_9) \quad \mathrm{cm^3\,mol^{-1}\,s^{-1}}. \tag{1}$$

The resonance strength $\omega\gamma$ of an isolated resonance for a (p,γ) reaction is given by

$$\omega\gamma = \frac{2J+1}{2(2j_t+1)}\frac{\Gamma_p\Gamma_\gamma}{\Gamma_{\mathrm{tot}}}, \tag{2}$$

where J and j_t are the spins of the resonance and the target nucleus, respectively, and the total width Γ_{tot} is the sum of the proton width Γ_p and the gamma width Γ_γ.

The proton width Γ_p can be estimated from the single-particle spectroscopic factor S and the single-particle width Γ_{sp} of the resonance by using [24]

$$\Gamma_p = C^2 S\Gamma_{\mathrm{sp}}, \tag{3}$$

where C is the isospin Clebsch-Gordan coefficient. The spectroscopic factors S are calculated in this work by using the nuclear shell model (Sec. III). Single-particle widths Γ_{sp} are obtained from resonant scattering phase shifts generated by an appropriate folding potential (see below). In this context, the partial width Γ_{sp} is defined as the energy interval over which the resonant phase shift varies from $\pi/4$ to $3\pi/4$.

Gamma widths for specific electromagnetic transitions are expressed in terms of reduced transition probabilities $B(J_i \rightarrow J_f;L)$ which contain the necessary nuclear structure information of the states involved in the transition [25]. The reduced transition probabilities can be calculated in the framework of the nuclear shell model. Alternatively they can be deduced from the experimentally known lifetimes of the corresponding states in the mirror nuclei. This method is used in this work (Sec. III). The total gamma width Γ_γ of a particular resonance is given by the sum over partial gamma widths for transitions to all possible lower-lying nuclear states.

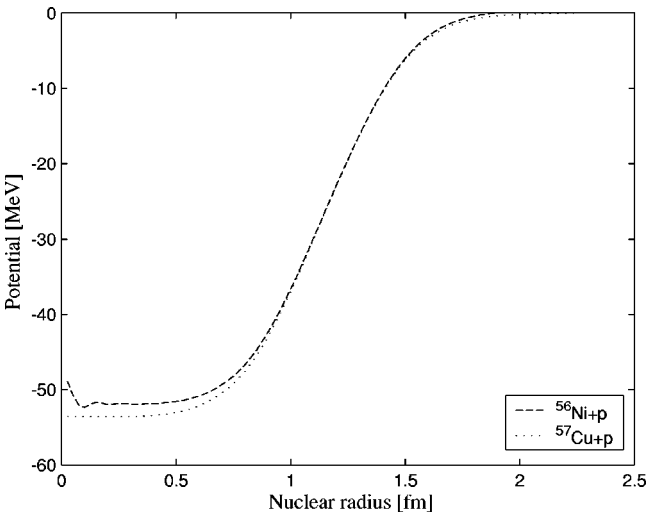

FIG. 1. Double folding potential used for the reaction ^{56}Ni$(p,\gamma)^{57}$Cu (dashed line) and for ^{57}Cu$(p,\gamma)^{58}$Zn (dotted line).

B. Nonresonant reaction contributions

The nonresonant proton capture cross section is calculated by using the direct capture (DC) model described in [26–28]. The DC cross section σ_i^{DC} for a particular transition is determined by the overlap of the scattering wave function in the entrance channel, the bound-state wave function in the exit channel and the electromagnetic multipole transition operator. Usually, only the dominant $E1$ transitions have to be taken into account. Wave functions are obtained by using a real folding potential given by [27,29]

$$V(R) = \lambda V_F(R) = \lambda\int\int \rho_a(\mathbf{r}_1)\rho_A(\mathbf{r}_2)v_{\mathrm{eff}}(E,\rho_a,\rho_A,s)d\mathbf{r}_1 d\mathbf{r}_2. \tag{4}$$

Here λ represents a potential strength parameter close to unity, and $s=|\mathbf{R}+\mathbf{r}_2-\mathbf{r}_1|$, with R the separation of the centers of mass of the projectile and the target nucleus. Since there exists no measured charge distributions [30] for ^{56}Ni and ^{57}Cu we used densities obtained using the Hartree-Fock method as described in Ref. [31]. The effective nucleon-nucleon interaction v_{eff} has been taken in the DDM3Y parametrization [29]. The imaginary part of the potential has been neglected due to the small flux into other reaction channels. The obtained real folding potential for the two reactions is shown in Fig. 1.

The total nonresonant cross section σ_{nr} is determined by summing contributions of direct capture transitions to all bound states with single-particle spectroscopic factors S_i:

$$\sigma_{\mathrm{nr}} = \sum_i (C^2S)_i\sigma_i^{\mathrm{DC}}. \tag{5}$$

TABLE I. Coulomb shifts δE_C, Thomas-Ehrman shifts δE_{TE}, and excitation energies E_x calculated for ^{57}Cu and ^{58}Zn. Excitation energies are given in MeV. Explanation in the text.

J^π	$E_x(^{57}\mathrm{Ni})$	δE_C	δE_{TE}	$E_x(^{57}\mathrm{Cu})$
$5/2^-$	0.77	0.061	0.16	0.99
J^π	$E_x(^{58}\mathrm{Ni})$	δE_C	$\delta E_{math\mathrm{TE}}$	$E_x(^{58}\mathrm{Zn})$
2_1^+	1.45	−0.051	−0.009	1.39
4_1^+	2.46	−0.010	0.11	2.55
2_2^+	2.78	−0.078	−0.001	2.70
1_1^+	2.90	−0.032	0.11	2.97
0_2^+	2.94	0.009	0.11	3.06
2_3^+	3.04	−0.060	0.062	3.04
2_4^+	3.26	−0.038	0.12	3.35
3_1^+	3.42	−0.051	0.12	3.49
0_3^+	3.53	−0.12	−0.027	3.39
1_2^+	3.59	−0.11	−0.068	3.42
3_2^+	3.77	−0.073	0.11	3.81

The astrophysical S factor of a charged-particle induced reaction is defined by [23]

$$S(E) = E \exp(2\pi\eta)\sigma(E), \tag{6}$$

with η denoting the Sommerfeld parameter. If the S factor depends only weakly on the bombarding energy the nonresonant reaction rate as a function of temperature T_9 can be expressed as

$$N_A\langle\sigma v\rangle_{\mathrm{nr}} = 7.833\times 10^9 \left(\frac{Z_1 Z_2}{A T_9^2}\right)^{1/3} S(E_0)[\mathrm{MeV\,b}] \times \exp\left[-4.249\left(\frac{Z_1^2 Z_2^2 A}{T_9}\right)^{1/3}\right] \quad \mathrm{cm^3\,mol^{-1}\,s^{-1}}, \tag{7}$$

with Z_1 and Z_2 the charges of the projectile and target, respectively, and A the reduced mass (in amu). The quantity E_0 denotes the position of the Gamow peak corresponding to the effective bombarding energy range of stellar burning.

TABLE II. Shell model spectroscopic factors of ^{57}Cu bound and unbound states.

		C^2S				λ	
E_x(MeV)	J^π	$2p_{1/2}$	$2p_{3/2}$	$1f_{5/2}$	$1f_{7/2}$	$l=p$	$l=f$
0.000	$3/2^-$		0.91				
1.028	$5/2^-$			0.91			0.99
1.106	$1/2^-$	0.90				1.03	
2.398	$5/2^-$			0.028[a]			0.95
2.520	$7/2^-$				0.01[a]		0.95

[a]From Zhou *et al.* [19].

TABLE III. Shell model spectroscopic factors of ^{58}Zn bound and unbound states.

		C^2S			λ	
E_x(MeV)	J^π	$2p_{1/2}$	$2p_{3/2}$	$1f_{5/2}$	$l=p$	$l=f$
0.000	0^+		1.20			
1.40	2^+	0.17	0.98	0.11		
2.55	4^+			0.95		0.99
2.70	2^+	0.16	0.99	0.22	1.02	0.98
2.97	1^+			1.0		0.98
3.04	2^+	0.29	0.023	0.64	1.0	0.97
3.06	0^+		0.79		1.0	
3.35	2^+	0.34	0.011	0.024	1.0	0.97
3.39	0^+		0.012		0.99	
3.42	1^+	1.0			0.99	
3.49	3^+			1.0		0.96
3.52	4^+			0.05[a]		0.96
3.56	4^+			0.05[a]		0.96
3.62	4^+			0.05[a]		0.96
3.81	3^+		1.0		0.98	

[a]Assumption.

III. EXPERIMENTAL AND THEORETICAL INPUT PARAMETERS

In this section we present a discussion of the excitation energies E_x, spectroscopic factors S, proton widths Γ_p, gamma widths Γ_γ, and resonance strengths $\omega\gamma$. We use the nuclear shell model to calculate excitation energies, Coulomb shifts and spectroscopic factors. The code OXBASH [32] has been employed for this purpose. We use the isospin–nonconserving (INC) interaction that has been developed by Ormand [22]. It is especially designed to describe the proton-rich isotopes in the mass range above ^{56}Ni.

The relevant excitation energies in ^{57}Cu have been measured by Zhou *et al.* [19]. For ^{58}Zn no experimental excitation energies are available. Therefore we use the known excitation energies in the mirror nucleus ^{58}Ni [33] and calculate Coulomb shifts in the shell model.

In the mass region above the double magic nucleus ^{56}Ni considerable Coulomb shifts between analogue states of mirror nuclei exist. The situation is similar to the mass region above the doubly magic nucleus ^{16}O. For some levels the strong shifts cannot be explained with the Coulomb shifts resulting from an INC interaction. This fact has been explained by the Thomas-Ehrman shift [34,35]. Since the proton single particle wave functions are only loosely bound, they are pushed out into the nuclear exterior. As a consequence the Coulomb energy is reduced. If two shell model orbits with different angular momenta are filled up different effects can occur. While in the region above ^{16}O the subshells $1d_{5/2}$ and $2s_{1/2}$ are filled up, in the region above ^{56}Ni a competition between the $2p_{3/2}$ and the $1f_{5/2}$ subshell takes place. However, in both cases the subshell with the lower angular momentum is pushed out much more and therefore experiences a smaller Coulomb energy.

We have used the method developed in Ref. [36] to cal-

TABLE IV. Resonance parameters for the reaction ^{56}Ni$(p,\gamma)^{57}$Cu.

E_x (keV)[a]	J_f^π	E_r (keV)[b]	Γ_p (eV)	Γ_γ (eV)	$\omega\gamma$ (eV)
1028	$5/2^-$	333	5.45×10^{-12}	3.55×10^{-4}	1.64×10^{-11}
1106	$1/2^-$	411	1.72×10^{-7}	4.23×10^{-3}	1.72×10^{-7}
2398	$5/2^-$	1703	9.13×10^{-2}	1.37×10^{-2}	3.57×10^{-2}
2520	$7/2^-$	1825	7.08×10^{-2}	8.38×10^{-3}	3.00×10^{-2}

[a]Experimental values adopted from Ref. [33].
[b]Calculated from column 1 and $Q_{p\gamma}=695$ keV [33].

culate the Thomas-Ehrman shifts for ^{57}Cu and ^{57}Ni as well as ^{58}Zn and ^{58}Ni. We have not taken into account possible complications due to the $2p_{1/2}$ subshell. In general the excited states have a stronger component of the $1f_{5/2}$-wave configuration than the ground state. Therefore the excited state of the proton-rich nucleus tends to be at a higher excitation energy than its analogue state. We have calculated the shifts for the excited states of ^{57}Cu and ^{58}Zn starting from their analogue states in ^{57}Ni and ^{58}Ni. The resulting Thomas-Ehrman shift δE_{TE} is then added to the Coulomb shift δE_{C} obtained from the shell model calculation with the INC interaction. The results are listed in Table I. We tested the method on the known first excited $5/2^-$ state in ^{57}Cu. Starting from the excitation energy of 768 keV in ^{57}Ni we calculated an excitation energy of 991 keV in the mirror nucleus, which is only 37 keV off the measured energy of 1028 keV (see Table I). This gives us confidence that we can also use this method for the calculation of the excitation energies of ^{58}Zn. Table I shows that all states experience relatively low shifts of not more than 170 keV.

The shifts for the second, third, and fourth excited state in ^{57}Cu are not included in Table I. The second excited $1/2^-$ state in ^{57}Cu is a good $2p_{1/2}$ single-particle state (see the discussion of the spectroscopic factors below). Since this subshell is not included in our model of the Thomas-Ehrman shift we did not calculate a shift for this state. The next two excited states ($5/2^-$ and $7/2^-$) are poorly described by the interaction and model space we have used [22]. However, the excited states of ^{58}Zn are well described in the model space which can be seen from the single particle spectroscopic factors.

The calculated spectroscopic factors are listed in Tables II and III. For the first two excited states in ^{57}Cu our shell model calculations agree with the experimental results of Rehm *et al.* [20]. For the third and fourth excited state of ^{57}Cu we use the spectroscopic factors given by Zhou *et al.* [19]. It will be interesting to investigate these spectroscopic factors with the larger model space and new effective interactions which are being developed for the fp shell [37].

In this work the gamma widths are deduced from the experimentally known lifetimes of the corresponding states in the mirror nuclei. We have corrected the transition energies using our adopted excitation energies and the well known energy dependence of the $E1$, $M1$, and $E2$ transitions. The obtained widths and resonance strengths are shown in Tables IV and V.

IV. RESULTS AND DISCUSSION

The resulting stellar rates of the ^{56}Ni$(p,\gamma)^{57}$Cu and ^{57}Cu$(p,\gamma)^{58}$Zn reaction can be parametrized for temperatures below $T_9=2$ by the expression [38]

TABLE V. Resonance parameters for the reaction ^{57}Cu$(p,\gamma)^{58}$Zn.

E_x (keV)[a]	J_f^π	E_R (keV)[b]	Γ_p (eV)	Γ_γ (eV)	$\omega\gamma$ (eV)
2554	4^+	274	8.65×10^{-15}	5.68×10^{-4}	9.73×10^{-15}
2697	2^+	417	7.71×10^{-8}	1.13×10^{-3}	4.82×10^{-8}
2971	1^+	691	5.65×10^{-6}	8.45×10^{-3}	2.12×10^{-6}
3040	2^+	760	1.9×10^{-3}	1.21×10^{-2}	1.02×10^{-3}
3057	0^+	777	6.75×10^{-3}	3.03×10^{-6}	3.78×10^{-7}
3349	2^+	1069	0.33	2.20×10^{-2}	1.29×10^{-2}
3389	0^+	1109	1.88×10^{-2}	1.92×10^{-3}	2.18×10^{-4}
3420	1^+	1140	2.22	1.12×10^{-2}	4.17×10^{-3}
3492	3^+	1212	3.13×10^{-2}	1.70×10^{-3}	1.41×10^{-3}
3524	4^+	1244	2.16×10^{-3}	6.88×10^{-3}	1.85×10^{-3}
3558	4^+	1278	3.24×10^{-3}	7.52×10^{-3}	2.55×10^{-4}
3620	4^+	1340	5.77×10^{-3}	3.31×10^{-3}	2.37×10^{-9}
3807	3^+	1527	4.45×10^{-3}	1.45×10^{-3}	9.55×10^{-4}

[a]Values taken from the last column of Table I.
[b]Calculated from column 1 and $Q_{p\gamma}=2280$ keV [33].

TABLE VI. Recommended parameters for the ^{56}Ni$(p,\gamma)^{57}$Cu reaction rate. [The total stellar reaction rate is given by Eq. (10).]

A_i	B_i	C	D
2.59×10^{-6}	3.86	2.21×10^{9}	39.3
2.72×10^{-2}	4.77		
5.65×10^{3}	19.8		
4.74×10^{3}	21.2		

$$N_A\langle\sigma v\rangle=\sum_i A_i/T_9^{3/2}\exp(-B_i/T_9) + C/T_9^{2/3}\exp(-D/T_9^{1/3})\ \ \mathrm{cm^3\,mol^{-1}\,s^{-1}}. \quad (8)$$

The first and second term in Eq. (8) represent the contributions of all narrow resonances and the direct capture process, respectively. The parameters A_i, B_i, C, and D are listed in Tables VI and VII.

The various contributions to the total reaction rates are displayed in Figs. 2 and 3. For both reactions the direct capture process can be neglected in the temperature range from $T_9=0.2$ to $T_9=2$. The ^{56}Ni$(p,\gamma)^{57}$Cu rate below 1 GK is clearly dominated by the resonant capture to the 1106 keV state. For higher temperatures the resonances of the 2398 keV and 2520 keV states determine the reaction rate. In the reaction ^{57}Cu$(p,\gamma)^{58}$Zn the three 2^+ resonances dominate the reaction rate.

We compare our ^{56}Ni$(p,\gamma)^{57}$Cu rate with the previous results in Fig. 4. Below a temperature of 1 GK our rate agrees with Rehm *et al.* [20] while it is about one order of magnitude larger than the rate of Zhou *et al.* [19] and up to two orders of magnitude larger than the rate of Van Wormer *et al.* [13]. In all calculations approximately the same spectroscopic factors (Van Wormer *et al.*: 0.8; Zhou *et al.*: 0.76; Rehm *et al.*: 0.9; this work: 0.9) have been used for the dominating $1/2^-$ resonance. The large discrepancies to the reaction rate of Zhou *et al.* is therefore only due to differences in the calculation of the penetrability. Our folding potential method agrees with the Woods-Saxon and *R*-matrix calculations performed by Rehm *et al.*, but gives a proton width one order of magnitude larger than the extended unified model (EUM) calculations of Zhou *et al.* Van Wormer *et al.* used another method to calculate the penetrability and different resonance energies. At higher temperatures (about 1.2 GK) the rates of Rehm *et al.* and Zhou *et al.* are almost identical because Rehm *et al.* used the resonance parameters from Zhou *et al.* for the 2398 and 2520 keV state. A slight difference remains as Rehm *et al.* made an additional approximation assuming $\Gamma_p\gg\Gamma_\gamma$ and consequently $\omega\gamma=\Gamma_\gamma$ for these states. Our rate is in this temperature regime about a factor of 2 smaller due to the smaller γ widths of these two states. We used the available experimental information from the mirror states to deduce the γ widths while Zhou *et al.* calculated them in the EUM.

TABLE VII. Recommended parameters for the ^{57}Cu$(p,\gamma)^{58}$Zn reaction rate. [The total stellar reaction rate is given by Eq. (10).]

A_i	B_i	C	D
1.54×10^{-9}	3.18	1.39×10^{9}	40.3
7.62×10^{-3}	4.84		
3.35×10^{-1}	8.02		
1.62×10^{2}	8.82		
5.98×10^{-2}	9.02		
2.04×10^{3}	12.4		
3.45×10^{1}	12.9		
6.60×10^{2}	13.2		
2.23×10^{2}	14.1		
2.93×10^{2}	14.4		
4.03×10^{2}	14.9		
3.74×10^{2}	15.6		
1.51×10^{2}	17.7		

In Fig. 5 our ^{57}Cu$(p,\gamma)^{58}$Zn rate is compared with the Hauser-Feshbach calculations using the code SMOKER [39,40]. The dashed line shows the old calculation based on a theoretical level density in ^{58}Zn and the dotted line shows a calculation using the new ^{58}Zn levels derived in the present work. According to Rauscher *et al.* [41] Hauser-Feshbach calculations for the ^{57}Cu$(p,\gamma)^{58}$Zn reaction rate are only reliable for $T_9>2.3$, because at lower temperatures the level density in ^{58}Zn is too small. Indeed below 2 GK both Hauser-Feshbach calculations give reaction rates that are an order of magnitude too low. As expected the results from the Hauser-Feshbach calculations are getting closer to our results at temperatures near 2 GK. Above 2 GK our reaction rate is smaller than the Hauser-Feshbach calculations because we did not include higher levels in our shell-model calculations. These results clearly demonstrate that Hauser-Feshbach calculations cannot be used to calculate the ^{57}Cu$(p,\gamma)^{58}$Zn reaction rate for most *rp* process temperatures. The criterion given by Rauscher *et al.* [41] seems to be reliable for the determination of the temperature range where the Hauser-Feshbach approach can be applied.

The dominating remaining uncertainties are for the

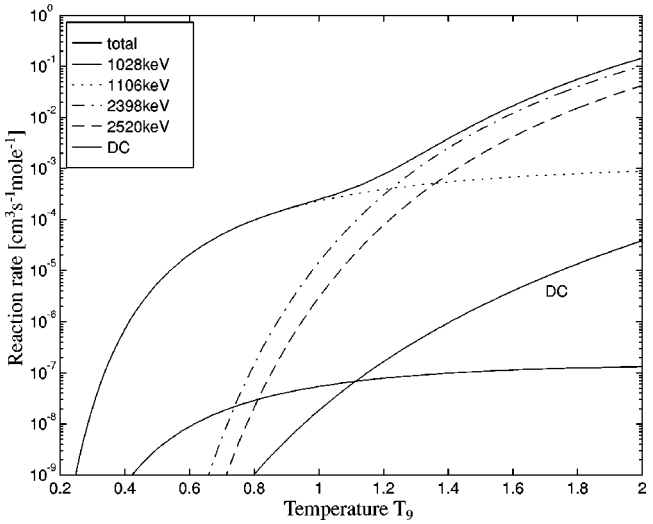

FIG. 2. Total stellar rate (solid line) and individual contributions (dashed lines) for the reaction ^{56}Ni$(p,\gamma)^{57}$Cu.

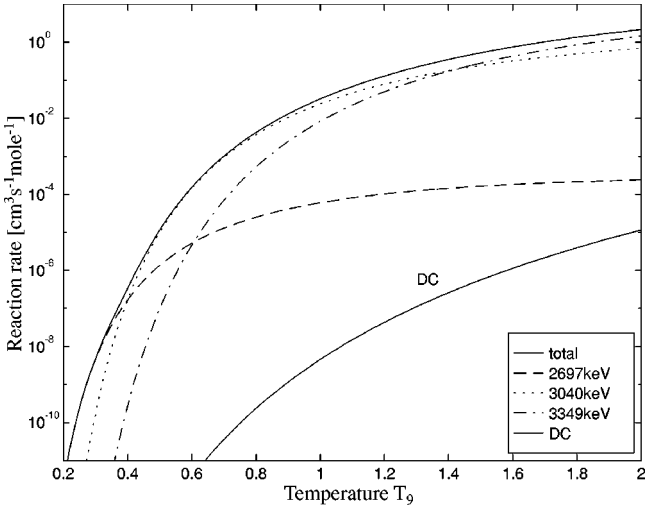

FIG. 3. Total stellar rate (solid line) and individual contributions (dashed lines) for the reaction ^{57}Cu$(p,\gamma)^{58}$Zn.

^{56}Ni$(p,\gamma)^{57}$Cu reaction the spectroscopic factors of the 2398 and 2520 keV states in ^{57}Cu. In ^{58}Zn some experimental information on excitation energies and spectroscopic factors of the 2^+ states would reduce the uncertainties. A non-negligible contribution to the rate uncertainties also comes from the experimental errors in the masses of ^{56}Ni (11 keV), ^{57}Cu (16 keV), and ^{58}Zn (50 keV) [42]. In Figs. 6 and 7 the Q-value dependence of the reaction rate is shown. The mass uncertainties have the strongest impact on the ^{56}Ni$(p,\gamma)^{57}$Cu rate below 1 GK, where the resulting uncertainty is up to a factor of 4. On the other hand, for the ^{57}Cu$(p,\gamma)^{58}$Zn rate the influence of mass uncertainties is very small. More precise mass measurements of ^{56}Ni and ^{57}Cu would be desirable.

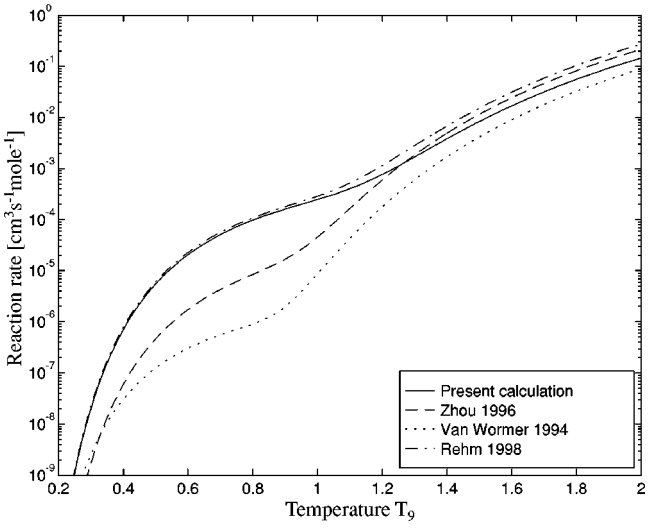

FIG. 4. Comparison of the present reaction rate for ^{56}Ni$(p,\gamma)^{57}$Cu to previous results of Zhou *et al.* [19] and Wormer *et al.* [13].

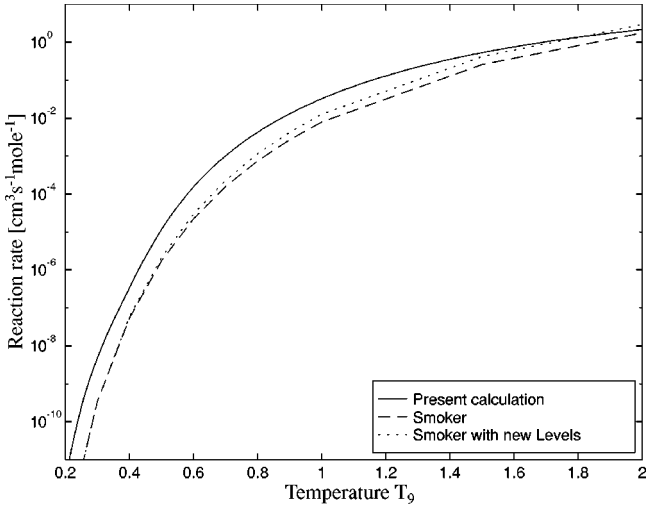

FIG. 5. Comparison of the present reaction rate for ^{57}Cu$(p,\gamma)^{58}$Zn to a previous calculation with the code SMOKER [39,40].

V. ASTROPHYSICAL IMPLICATIONS

The new ^{56}Ni$(p,\gamma)^{57}$Cu and ^{57}Cu$(p,\gamma)^{58}$Zn reaction rates allow us now to recalculate the effective rp-process half-life of ^{56}Ni against proton and electron capture. This was done by solving the differential equations describing the abundance of ^{56}Ni as a function of time for a fixed temperature and density and calculating the time required to reduce the ^{56}Ni abundance to half of its initial value. This represents a small reaction network including all reactions that affect the ^{56}Ni lifetime, which are proton captures on ^{56}Ni and ^{57}Cu, (γ,p) photodisintegration of ^{58}Zn, ^{57}Cu, and ^{56}Ni, as well as continuum electron capture on ^{56}Ni (which turns out to be negligible) and β decays of ^{57}Cu and ^{58}Zn. The reaction rates used besides the new proton capture reaction rates on ^{56}Ni and ^{57}Cu discussed in this work were described in detail in Van Wormer *et al.* [13]. All calculations were per-

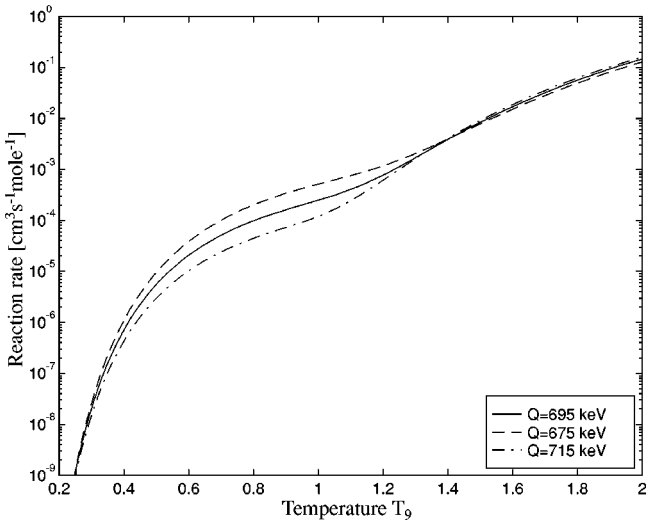

FIG. 6. Dependence of the reaction rate for ^{56}Ni$(p,\gamma)^{57}$Cu on the Q value.

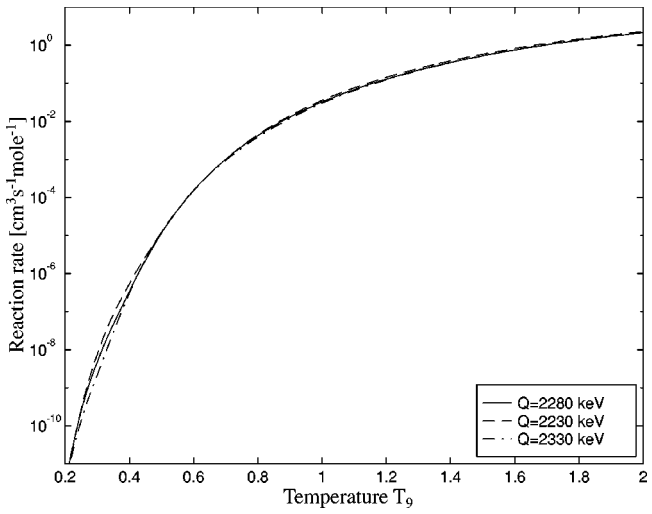

FIG. 7. Dependence of the reaction rate for ^{57}Cu$(p,\gamma)^{58}$Zn on the Q value.

formed for solar hydrogen abundance. The result is shown in Fig. 8 as a function of temperature and at a fixed density of 10^6 g/cm^3, which is typical for x-ray bursts and x-ray pulsars. Screening has been taken into account according to Refs. [43,44]. For comparison, Fig. 8 also shows the same calculation based on the frequently used rate of Van Wormer

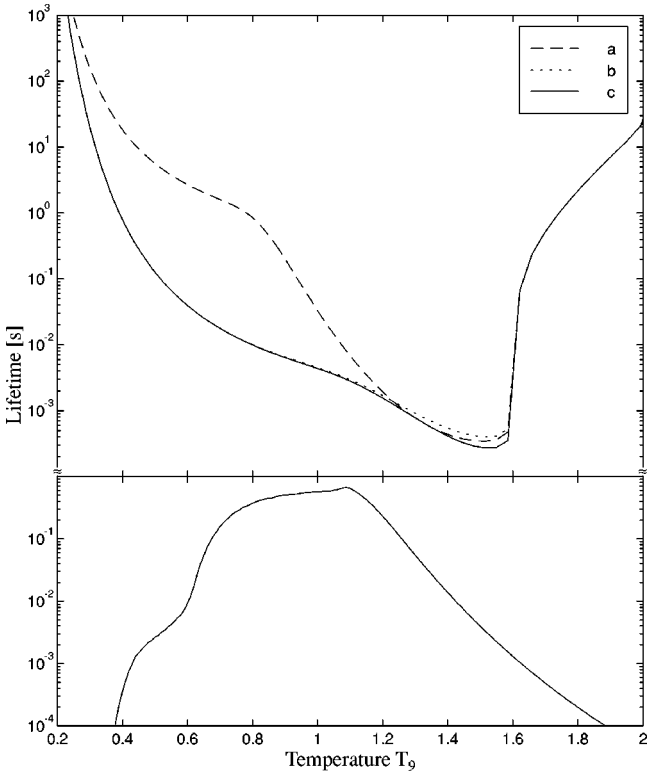

FIG. 8. Upper panel: Lifetime of ^{56}Ni: (a) ^{56}Ni$(p,\gamma)^{57}$Cu rate taken from Van Wormer *et al.* [13] and ^{57}Cu$(p,\gamma)^{58}$Zn rate taken from Hauser-Feshbach calculations [39,40]; (b) new ^{56}Ni$(p,\gamma)^{57}$Cu rate and ^{57}Cu$(p,\gamma)^{58}$Zn rate taken from Hauser-Feshbach calculations [39,40]; (c) new ^{56}Ni$(p,\gamma)^{57}$Cu rate and new ^{57}Cu$(p,\gamma)^{58}$Zn rate. Lower panel: ^{55}Ni bypass.

et al. [13] and, to demonstrate the influence of the different reactions, also for the new ^{56}Ni$(p,\gamma)^{57}$Cu reaction rate together with the old Hauser-Feshbach rate for ^{57}Cu$(p,\gamma)^{58}$Zn. For temperatures between 0.35 and 0.95 GK the new ^{56}Ni$(p,\gamma)^{57}$Cu rate leads to a reduction of the ^{56}Ni lifetime by 1–2 orders of magnitude. However, for the interpretation of the consequences for the rp process it has to be taken into account that there is a possibility of bypassing ^{56}Ni via the ^{55}Ni$(p,\gamma)^{56}$Cu$(p,\gamma)^{57}$Zn$(\beta^+)^{57}$Cu reaction sequence for temperatures between 0.65 and 1.1 GK (bypass $>50\%$—see the lower panel of Fig. 8). For this temperature range the ^{56}Ni lifetime has no strong impact on the rp process. However, the calculations for this bypass sequence are quite uncertain and based on the theoretical mass predictions of Ormand [22]. An experimental determination of the ^{56}Cu mass would be very important.

At higher temperatures the ^{56}Ni$(p,\gamma)^{57}$Cu reaction is very fast, but (γ,p) photodisintegration of the relatively weakly proton-bound ^{57}Cu hampers effective proton captures leading again to higher lifetimes. Two cases have to be distinguished. (1) as long as photodisintegration on the more proton bound ^{58}Zn does not play a role, there is a (p,γ)-(γ,p) equilibrium established between ^{56}Ni and ^{57}Cu, but not between ^{57}Cu and ^{58}Zn. Then the lifetime of ^{56}Ni depends on the mass difference between ^{56}Ni and ^{57}Cu and the ^{57}Cu$(p,\gamma)^{58}$Zn reaction rate. (2) However, above the temperature where photodisintegration on ^{58}Zn starts playing a role, ^{56}Ni, ^{57}Cu, and ^{58}Zn are in (p,γ)-(γ,p) equilibrium and then the ^{56}Ni lifetime depends not on the ^{57}Cu$(p,\gamma)^{58}$Zn reaction rate anymore, but on the mass difference between ^{56}Ni and ^{58}Zn and the β^+ decay rate of ^{58}Zn. It turns out that because the new ^{57}Cu$(p,\gamma)^{58}$Zn is so large, case (2) sets in at a lower temperature than case (1) despite of the fact that ^{58}Zn is more proton bound. This happens because as a consequence of the detailed balance principle a higher ^{57}Cu$(p,\gamma)^{58}$Zn reaction rate means also a higher ^{58}Zn photodisintegration rate. Therefore, photodisintegration of ^{58}Zn sets already in at lower temperatures [case (2)], while at the same time photodisintegration of ^{57}Cu requires higher temperatures to compete with the increased proton capture rate [case (1)]. Above a certain ^{57}Cu$(p,\gamma)^{58}$Zn rate the temperature conditions for the onset of case (1) and (2) crossover, and case (1) is skipped. Therefore, with the new ^{57}Cu$(p,\gamma)^{58}$Zn reaction rate it can be concluded that its not the ^{57}Cu$(p,\gamma)^{58}$Zn reaction rate but the β^+ decay rate of ^{58}Zn that determines the ^{56}Ni lifetime against proton capture at high temperatures. This is illustrated in Fig. 8, which shows that there is hardly any difference in the ^{56}Ni lifetime calculated with the old and with the new ^{57}Cu$(p,\gamma)^{58}$Zn reaction rate. The possible influence of the new ^{56}Ni lifetime against proton capture on the rp process in x-ray bursts and x-ray pulsars is discussed in the following.

In x-ray bursts the important question is whether the rp process can proceed beyond ^{56}Ni within the typical burst time scale of 10 s. Figure 8 shows that there is indeed a temperature window around 1 GK, where the lifetime of ^{56}Ni is below 10 s. The new reaction rates enlarge this window considerably and it ranges now from 0.33 to 1.95 GK

(instead of 0.45–1.9 GK with the Van Wormer *et al.* [13] rates). Therefore the previously made conclusions remain unchanged that for typical burst peak temperatures of 1–2 GK the *rp* process can well proceed beyond ^{56}Ni. However, the time during cooling where nuclei above ^{56}Ni can be produced becomes significantly longer. This will be especially important for short bursts, where the fraction of material getting stuck at ^{56}Ni will be reduced. An important new aspect is that with the new reaction rates the temperature threshold for *rp* processing beyond ^{56}Ni coincides roughly with the temperature limit for the breakout of the CNO cycle. So any burst that will be hot enough for the *rp* process to occur will also be hot enough for processing beyond ^{56}Ni. For bursts with peak temperatures near 2 GK the *rp* process gets stuck in ^{56}Ni until temperatures cool down to reach again a ^{56}Ni lifetime of around 10 s. The temperature where this happens sets the temperature for the *rp* process beyond ^{56}Ni. As discussed above, it is now clear from the new ^{57}Cu$(p,\gamma)^{58}$Zn reaction rate that this temperature is not determined by the ^{57}Cu$(p,\gamma)^{58}$Zn reaction, but by the ^{58}Zn β^+ decay rate.

In x-ray pulsars hydrogen and helium are burned in steady state and the *rp* process will end when all the hydrogen is consumed. An important question is how much ^{56}Ni is produced in these scenarios. Older studies assumed that ^{56}Ni is the sole product of the nucleosynthesis and all theoretical descriptions used this as a starting point. Schatz *et al.* [17,18] showed that this is not the case and that depending on the accretion rate a variety of nuclei between $A=50-100$ are made. However, they still found an appreciable amount of ^{56}Ni in the final composition of the *rp*-process ashes. This is due to the long lifetime (of the order of seconds and more) for ^{56}Ni for temperatures below 1 GK, which make ^{56}Ni a waiting point. The abundance accumulated at a waiting point is roughly proportional to its lifetime. Therefore, with the new reaction rates, the final ^{56}Ni abundance will be reduced by a factor of 10–100 (see Fig. 8). With our new rates the conclusion will most likely be that there is no ^{56}Ni produced at all in x-ray pulsars.

Finally, we give in Fig. 9 the lifetime of ^{56}Ni against proton capture as a function of temperature and density based on the new reaction rates. This plot can be read as the processing time that is needed for the *rp* process to get beyond ^{56}Ni for a given temperature and density condition. Of course this is a lower limit and the time for the *rp* process to reach ^{56}Ni has to be added.

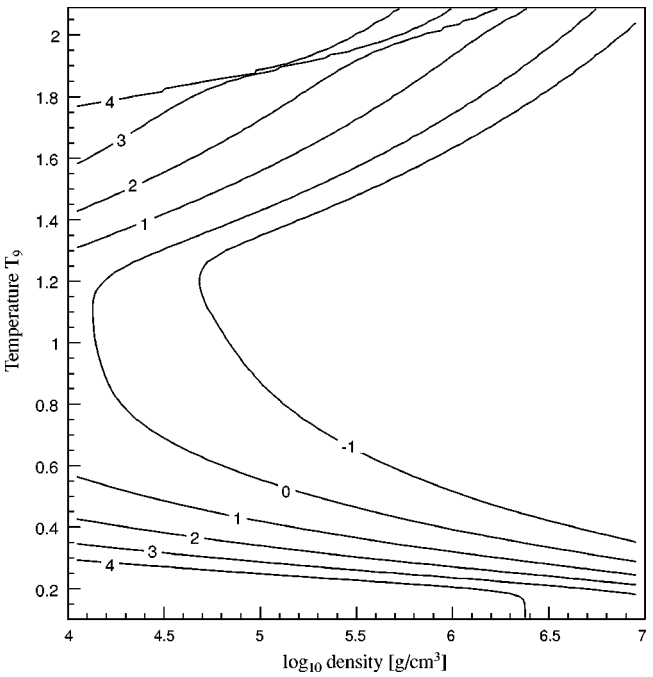

FIG. 9. Lifetime of ^{56}Ni in the *rp* process as a function of temperature and density. The contour level labels indicate the $\log_{10}$ of the lifetime in seconds. The ^{56}Ni lifetime is mainly determined by proton captures, and a solar hydrogen abundance has been assumed.

VI. SUMMARY AND CONCLUSIONS

The energy shift of the first excited $5/2^-$ state in ^{57}Cu has been calculated from the corresponding state of ^{57}Ni with the help of the Coulomb and Thomas-Ehrmann shifts. Excellent agreement with the experimentally obtained energy shift is obtained. In an analogous way using again the Coulomb and Thomas-Ehrmann shifts the excitation energies and spin/parity assignments of the experimentally unknown levels of ^{58}Zn were obtained. The proton and gamma widths of the astrophysically relevant resonances are estimated with the help of shell model calculations. With these consistent experimental and theoretical input parameters the reaction rates for ^{56}Ni$(p,\gamma)^{57}$Cu and ^{57}Cu$(p,\gamma)^{58}$Zn have been calculated. The results confirm the new ^{56}Ni$(p,\gamma)^{57}$Cu reaction rate given recently by Rehm *et al.* [20] for temperatures below 1 GK and lead to a significantly improved rate at higher temperatures. Compared with reaction rates previously used in astrophysical network calculations, this new rate drastically changes the lifetime of ^{56}Ni against proton capture in the *rp* process and reduces the minimum temperature required for the *rp* process to proceed beyond ^{56}Ni. For x-ray burst densities this minimum temperature coincides now with the temperature for the break out of the hot CNO cycles. We also present the first reliable calculation of the ^{57}Cu$(p,\gamma)^{58}$Zn reaction rate. Based on this new rate we can now conclude that it is in fact not the ^{57}Cu$(p,\gamma)^{58}$Zn reaction rate but the ^{58}Zn β^+ decay rate that determines the ^{56}Ni lifetime in the *rp* process at high temperatures.

ACKNOWLEDGMENTS

We would like to thank T. Rauscher for providing the latest Hauser-Feshbach calculations for the ^{57}Cu$(p,\gamma)^{58}$Zn reaction rate and F.-K. Thielemann for supplying the reaction network code used for the calculation of the ^{56}Ni lifetime. This work was supported by Fonds zur Förderung der Wissenschaftlichen Forschung in Österreich (Project No. S7307-AST). B.A.B. is supported by NSF Grant No. PHY-9605207.

[1] R. K. Wallace and S. E. Woosley, Astrophys. J., Suppl. Ser. **45**, 389 (1981).
[2] M. Politano, S. Starrfield, J. W. Truran, A. Weiss, and W. M. Sparks, Astrophys. J. **448**, 807 (1995).
[3] R. E. Taam, S. E. Woosley, and D. Q. Lamb, Astrophys. J. **459**, 271 (1996).
[4] L. Jin, W. D. Arnett, and S. K. Chakrabarti, Astrophys. J. **336**, 572 (1989).
[5] Karlsruher Nuklidkarte, 6. Auflage 1995.
[6] B. Sur, E. B. Norman, K. T. Lesko, E. Browne, and R.-M. Larimer, Phys. Rev. C **42**, 573 (1990).
[7] G. M. Fuller, W. A. Fowler, and M. J. Newman, Astrophys. J., Suppl. **42**, 447 (1980).
[8] S. E. Woosley and T. A. Weaver, in *High Energy Transients in Astrophysics*, edited by S. E. Woosley, AIP Conf. Proc. No. 115 (American Institute of Physics, New York, 1984), p. 273.
[9] R. E. Taam, S. E. Woosley, T. A. Weaver, and D. Q. Lamb, Astrophys. J. **413**, 324 (1993).
[10] R. E. Taam, S. E. Woosley, and D. Q. Lamb, Astrophys. J. **459**, 271 (1996).
[11] R. K. Wallace and S. E. Woosley, in *High Energy Transients in Astrophysics* (Ref. [8]), p. 319.
[12] T. Hanawa, D. Sugimoto, and M. A. Hashimoto, Publ. Astron. Soc. Jpn. **35**, 491 (1983).
[13] L. van Wormer, J. Görres, C. Iliadis, M. Wiescher, and F.-K. Thielemann, Astrophys. J. **432**, 326 (1994).
[14] O. Koike, M. Hashimoto, K. Arai, and S. Wanajo, Astron. Astrophys. **342**, 464 (1999).
[15] *Intersections between Particle and Nuclear Physics*, edited by H. Schatz, L. Bildsten, J. Görres, F.-K. Thielemann, M. Wiescher, and T. W. Donnelly, 6th Conference, Big Sky, Montana, AIP Conf. Proc. No. 412 (American Institute of Physics, New York, 1997), p. 987.
[16] H. Schatz, A. Aprahamian, J. Görres, M. Wiescher, T. Rauscher, J. F. Rembges, F.-K. Thielemann, B. Pfeiffer, P. Möller, K.-L. Kratz, H. Herndl, B. A. Brown, and H. Rebel, Phys. Rep. **294**, 1 (1998).
[17] H. Schatz, L. Bildsten, A. Cumming, and M. Wiescher, in Nuclei in the Cosmos V, edited by N. Prantzos, Volos, Greece, 1998 (in press).
[18] H. Schatz, L. Bildsten, A. Cumming, and M. Wiescher, Astrophys. J. **524**, 1014 (1999).
[19] X. G. Zhou *et al.*, Phys. Rev. C **53**, 982 (1996).
[20] K. E. Rehm *et al.*, Phys. Rev. Lett. **80**, 676 (1998).
[21] F.-K. Thielemann (private communication).
[22] W. E. Ormand, Phys. Rev. C **55**, 2407 (1997).
[23] C. E. Rolfs and W. S. Rodney, *Cauldrons in the Cosmos* (The University of Chicago Press, Chicago, 1988).
[24] J. P. Schiffer, Nucl. Phys. **46**, 246 (1963).
[25] P. J. Brussaard and P. W. M. Glaudemans, *Shell-Model Applications in Nuclear Spectroscopy* (North-Holland, Amsterdam, 1977).
[26] K. H. Kim, M. H. Park, and B. T. Kim, Phys. Rev. C **35**, 363 (1987).
[27] H. Oberhummer and G. Staudt, in *Nuclei in the Cosmos*, edited by H. Oberhummer (Springer-Verlag, Berlin, New York, 1991), p. 29.
[28] P. Mohr, H. Abele, R. Zwiebel, G. Staudt, H. Krauss, H. Oberhummer, A. Denker, J. W. Hammer, and G. Wolf, Phys. Rev. C **48**, 1420 (1993).
[29] A. M. Kobos, B. A. Brown, R. Lindsay, and G. R. Satchler, Nucl. Phys. **A425**, 205 (1984).
[30] H. de Vries, C. W. de Jager, and C. de Vries, At. Data Nucl. Data Tables **36**, 495 (1987).
[31] J. Street, B. A. Brown, and P. E. Hodgson, J. Phys. G **8**, 839 (1982).
[32] B. A. Brown, A. Etchegoyen, W. D. M. Rae, and N. S. Godwin, code OXBASH, 1984 (unpublished).
[33] R. B. Firestone, *Table of Isotopes*, 8th ed. (Wiley, New York, 1996).
[34] R. F. Thomas, Phys. Rev. **81**, 148 (1951).
[35] J. B. Ehrman, Phys. Rev. **81**, 412 (1951).
[36] H. Herndl, J. Görres, M. Wiescher, B. A. Brown, and L. van Wormer, Phys. Rev. C **52**, 1078 (1995).
[37] T. Mizusaki, T. Otsuka, Y. Utsuno, M. Honma, and T. Sebe, Phys. Rev. C **59**, 1846 (1999); E. Caurier, G. Martinez-Pinedo, F. Nowacki, A. Poves, J. Retamosa, and A. P. Zuker, *ibid.* **59**, 2033 (1999).
[38] M. Wiescher, J. Görres, F.-K. Thielemann, and H. Ritter, Astron. Astrophys. **160**, 56 (1986).
[39] F.-K. Thielemann *et al.*, *Advances in Nuclear Astrophysics* (Editions Frontiéres, Gif-sur-Yvette, 1987), p. 525.
[40] J. J. Cowan, F.-K. Thielemann, and J. W. Truran, Phys. Rep. **208**, 268 (1991).
[41] T. Rauscher, F.-K. Thielemann, and K.-L. Kratz, Phys. Rev. C **56**, 1613 (1997).
[42] G. Audi and A. H. Wapstra, Nucl. Phys. **A595**, 409 (1995).
[43] H. C. Graboske, H. E. DeWitt, A. S. Grossman, and M. S. Cooper, Astrophys. J. **181**, 457 (1973).
[44] N. Itoh, H. Totsuji, S. Ichimaru, and H. E. DeWitt, Astrophys. J. **234**, 1079 (1979).